The use of POD filtering to study the transition from 2D to 3D in stratified two-phase flow

Hann, David. B.[1*], Loizou, Katerina[2], Vasques, Joao, C.[1], Tokarev, Mikhail.P.[3,4], Cherdantsev, Andrey. V.[3,4]
1: University of Nottingham, UK,
2: University College, London, UK,
3: Kutateladze Institute of Thermophysics, Novosibirsk, Russia,
4: Novosibirsk State University, Novosibirsk, Russia
* Correspondent author: david.hann@nottingham.ac.uk

Keywords: PIV processing, two-phase sheared flow, POD

ABSTRACT

The understanding of the velocity profile beneath waves in sheared flow can have implications for the understanding of heat transfer in many applications. In this paper an analysis of the velocity field beneath 2D and 3D waves is performed to understand the differences in the behavior. A drop in the average wall shear stress is identified when the gas flow rate increases past 3m/s and the flow transitions from 2D to 3D waves. POD filtering is employed to reconstruct the PIV series and remove much of the PIV processing noise to aid in the understanding of higher order statistics. Filtering levels were put at between 90-97% depending on the flow situation. It is demonstrated that in the 3D case, the instantaneous wall shear stress can be negative despite a positive average value leading to circulations beneath the trough. There is enhanced interfacial shear above the crest and this could lead to the flow reversal due to continuity. Some further turbulent statistics are considered to see the effect of the POD filtering on the results and there appears to be some promise in that approach, although further work will need to be done to ascertain the exact impact.

1. Introduction

Steady stratified two-phase flow occurs when the velocity of each phase is relatively low. As the gas flow rate increases, instabilities at the interface cause capillary waves that initially are 2D linear structures such as those shown in Figure 1a. As the gas flow rate is further increased, the transverse length of these capillary waves decreases and the surface waves have a more 3D structure. One of the key variables for the predictors of the flow regime is the wall shear stress which is the main variable for calculation of the friction velocity. This can be estimated by measurement of the velocity profile in the liquid layer close to the wall and understanding of this parameter can aid in the understanding of the physical mechanisms which cause the transition from the 2D to 3D flow regime.

The measurement of velocity in thin gas-sheared films has a number of challenges. Schubring et al. (2009) was one of the first to apply PIV to this challenging application. This was followed by measurements in horizontal stratified pipe flow by Ayati et al. (2014, 2015) and inclined falling films and shear driven film in vertical pipes (Zadrazil and Markides, 2014).

Ashwood et al. (2015) applied PIV in thin planes parallel to the wall to estimate the average profiles in co-current flow vertically upwards in a rectangular duct. This work demonstrated that the Universal Velocity Profile of a single phase flow did not fit when the flow was stratified. Cioncolini et al. (2015) reanalysed this data and came to a similar conclusion. In single phase fluids the laminar region extends to $y^+ \approx 5$, where $y^+ = \frac{y u_\tau}{\nu}$, and the friction velocity is related to the velocity gradient by $u_\tau = \sqrt{\frac{\mu}{\rho}\frac{\partial u}{\partial y}\Big|_{y=0}}$. Cioncolini et al. (2015) demonstrated that the laminar region extended to $y^+ \approx 9$ for two-phase flows, meaning that the turbulence in the liquid film does not reach as close to the channel wall as it does in corresponding turbulence in single phase boundaries. This suggest caution for those using the single phase boundary condition for the prediction of corresponding heat transfer coefficients since these will tend to be over predictions. So further work in the understanding of the turbulent boundary layer in two-phase flow is essential for improvements in CFD models of multiphase heat exchangers such as those in steam or nuclear powered steam generators.

André and Bardet (2015); Ayati et al. (2015) both looked at measurements of the gas and liquid phase to obtain details of the interface. Understanding this is vital to validating CFD codes. The work presented here is the first stage in a campaign to repeat this for geometries and flow situations more relevant for aircraft engine cooling. In this paper the transition from the 2D to the 3D flow regime is considered using PIV.

a

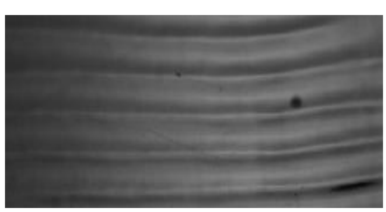

b

Fig. 1 Showing the comparison of (a) 2D and (b) 3D waves measured in the rectangular duct.

In the present apparatus, at velocities of approximately 3 m/s, the sheared surface of the liquid transitions from linear waves that span over the width, to "pebble dashed" waves which are finite in width (Fig 1).

Proper Orthogonal Decomposition

The PIV maps contain a large dynamic range of velocities meaning that to obtain the largest velocities near the surface, it is necessary to have significant PIV generated noise at the lower velocity near the wall. However, the wall is the region of interest. It was noted that the flow oscillations are regular and quasi-stationary, so a POD technique similar to that adopted by Wee (2015) which separated acoustically generated turbulence from a non-linear acoustic wave was implemented. The concept of using POD filtering for PIV noise removal is not new. It was first implement by Graftieaux et al. (2001) to identify the location of an unsteady swirling flow and there are many examples of its use in the literature(for example there are 403 documents that cite this paper alone). Similarly, Perrin et al. (2007) used a POD technique as a filter to obtain turbulent properties. The use of POD for determination of phase averaged and statistical properties might provide a more faithful indication of the evolution of the coherent structures than phase averaging and Reynolds averaging (Ma and Schröder, 2017).

The premise of the Proper Orthogonal Decomposition is that N instantaneous velocity fields can be decomposed into N linear modes that can be partially or fully recombined to produce either approximations or the original data set. Each of these modes is associated with a series of coefficients that are used in the reconstruction. The modes are empirical and might or might not be associated with a physical mechanism in the flow. In our experience an acoustic mode of one frequency has 2 energetic modes. If two frequencies are present, then there are four energetic modes and if three frequencies are present then there are 2^3energetic modes. In situations where the flow is complex, with multiple components, this means that there are sometimes too many modes of interest for clear understanding with the POD technique. This is also true when the flow is not statistically stationary and the repetition of a flow pattern is occasional. The modes in POD are ranked by energy, and it is possible to filter out the least energetic modes and reconstruct with modes with an energy of the order of 90-95% so that large scale motions, or significant gradients of the flow can be understood more clearly.

2. Methodology

Results for this paper were taken in a horizontal rectangular duct of cross section (H=0.025 m, W=0.161m (see Fig 2.)). The liquid was introduced by a pump into a manifold at the inlet and a shearing air flow generated by a compressor and conditioned by a honeycomb section was used to drive the flow along the duct to the measurement location which was 1.5 m from the inlet (about $37D_h$) at which point it may be considered a fully developed flow (Cherdantsev et al., 2014). PIV measurements were taken through the side wall of the duct of the thin film at a plane in the centre of the duct. The film was approximately 3mm in height for the flow parameters under investigation so a 26 m x 4 mm area was viewed with the camera. Two Liquid Reynolds numbers of 166 and 207 were investigated for gas velocities ranging from 2-3.2 m/s which corresponded to

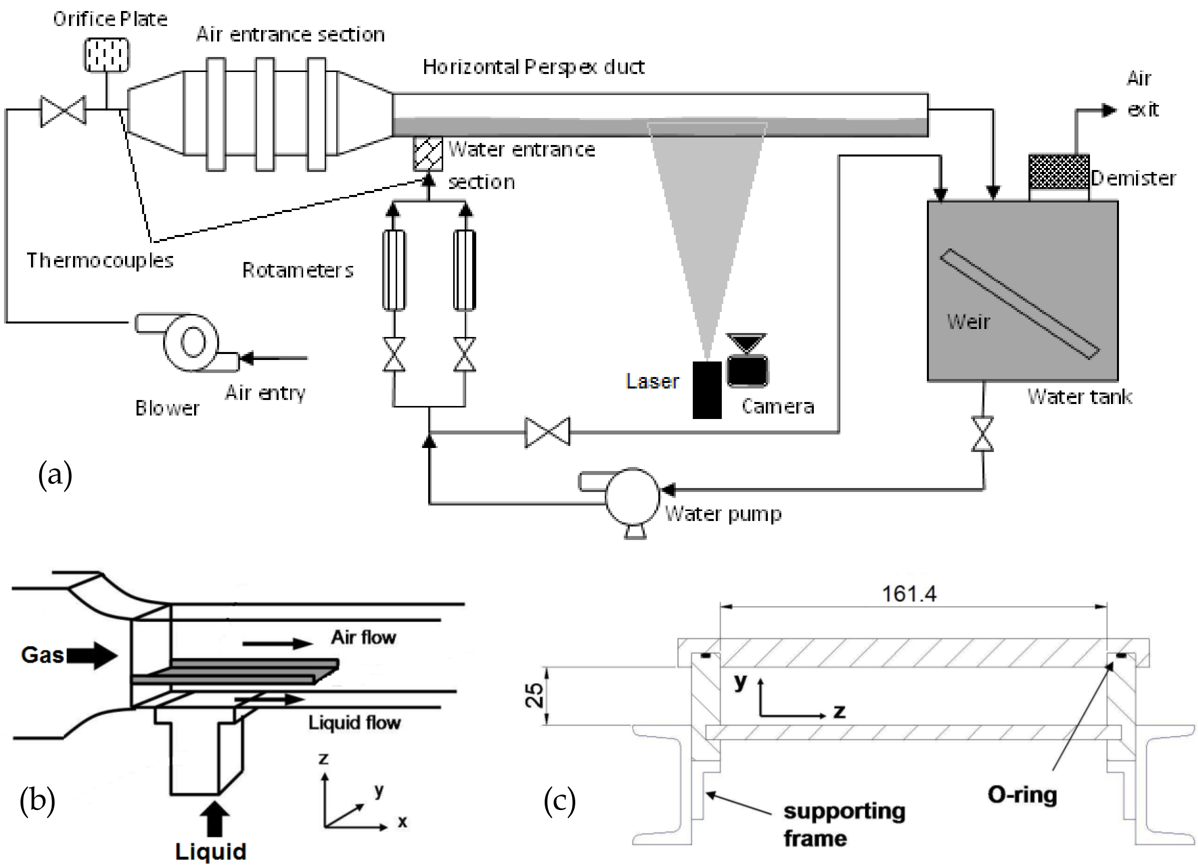

Fig 2. (a) Schematic of the apparatus for the PIV, (b) schematic of air/liquid manifold (c) Dimensions of the duct cross section. For these experiments, the liquid was water and the gas was air.

the observed transition from 2D to 3D flow in the duct. The resolution of the imaging was 20.5 microns/pixel and 2000 images were taken at 500 Hz. The individual images were processed in Matlab to identify the surface which allowed an individual mask to be generated for each image and a median filter was applied to decrease background noise before processing. The processed images were then loaded in the DANTEC Dynamic studio program to calculate velocity fields using a multi-pass PIV algorithm. The air flow was measured using a calibrated orifice plate connected to a differential pressure transducer to within 1%. The liquid in this case was tap water and was monitored with a variable area flowmeter.

3. Results

3.1 Unprocessed results

In the flow regime of interest, there are two main flow types present and there is a transition expected at about 3.0 m/s. Fig 3. and 4. show the PIV results for the case of Re=207 and v_g =3.0 and 3.2 m/s respectively. As can be seen, the PIV maps are noisy, but animation shows that the high vorticity near the wall at the rear of Fig 4 moves through the region and is therefore significant and not an artefact of the PIV noise. It is also clear that there is significant noise in the gradient of the velocity due to the uncertainties in the PIV process. The overlaid vorticity (calculated from the 2D components) is inherently noisy and any underlying large features are obscured.

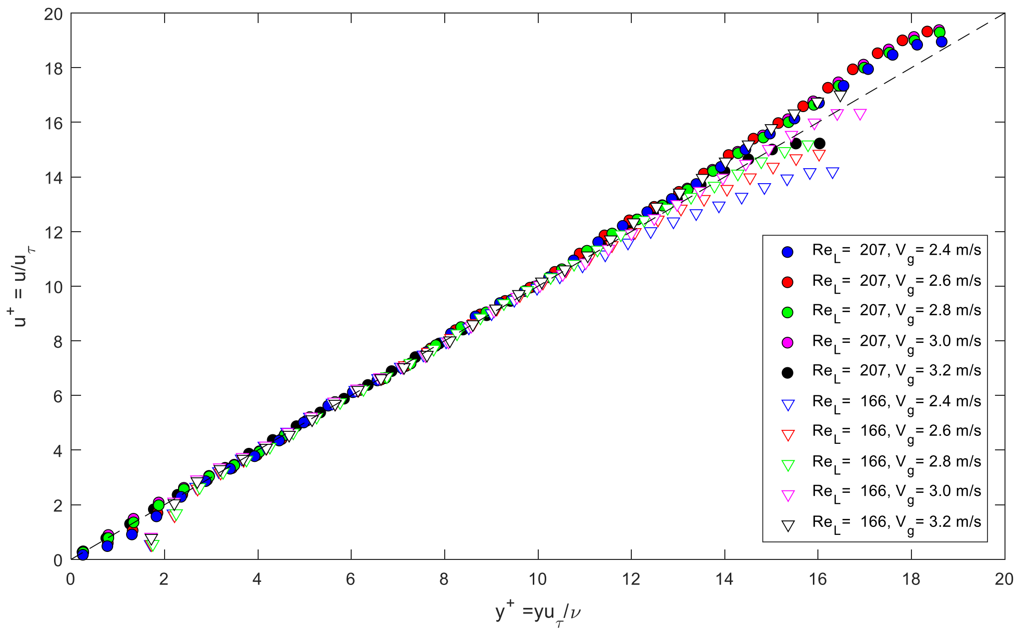

d.

Only every second PIV vector is displayed. (b) Velocity profiles at lines indicated in (a). Note vertical

Fig. 5: Average velocity beneath the waves for all cases normalised using law of the wall units. The linear region extends to $y^{+}{\sim}10$.

a): Original vector map with vorticity: V = 3.2 m/s

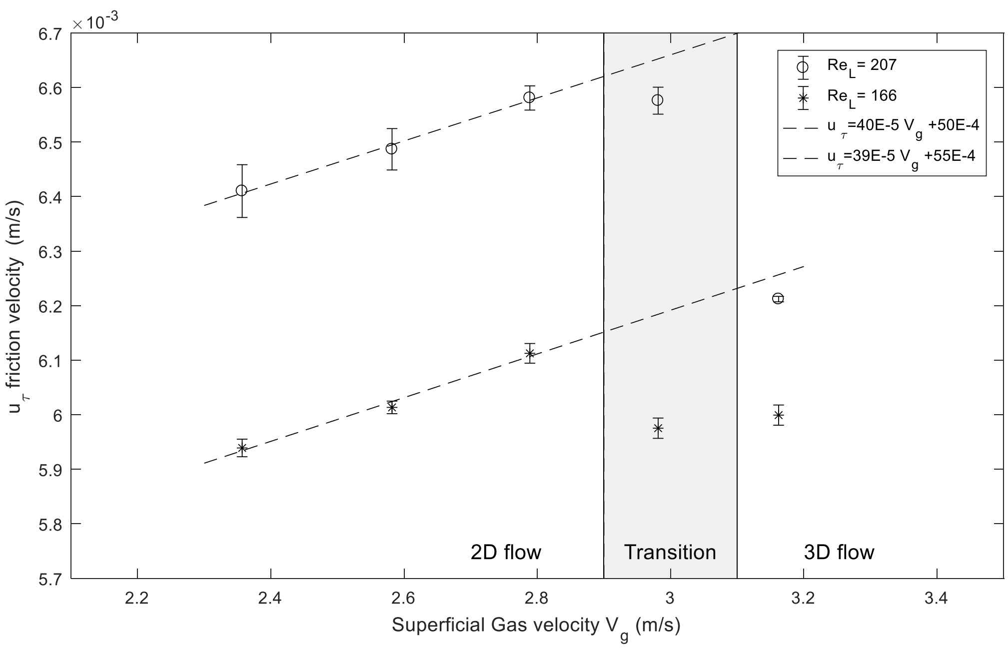

id.
is a
ity

Fig. 6: The measured friction velocity for the two Reynolds numbers measured. Error bars are the 95% confidence level of the curve fit for the local wall gradient. There is a clear change in behaviour at around 3 m/s.

Despite this, there is a clear change in the behaviour of the waves and the pattern fits with the transition from 2D (Fig. 3) to 3D (Fig. 4) waves for constant liquid flow as the air velocity increases from 3.0 to 3.2 m/s. In Fig. 3 the surface has only a small variation in height, while in Fig. 4, the surface height varies more significantly. The possible high vorticity region near the wall in Fig. 4 occurs at the trough of the wave at X~8 mm. Despite the potential reversal apparent in Fig 4, the average velocity profiles are linear close to the wall. It is possible to determine the local average gradients at the wall and to use this to determine the wall shear stress $\tau_w = \mu \frac{du}{dx}\Big|_{x=0}$. The averaged velocity profiles can then be shown to be self-similar as expected in the laminar region close to the wall. According to classical boundary layer theory, the linear region extends to $y^+ = 5$. However this result agrees with Cioncolini et al. (2015) and Ashwood et al. (2015) to show that in sheared wavy flow, the laminar region extends to $y^+ \sim 10$, despite the difference in orientation of the flow. The Ashwood results are for vertical upward annular flow in a circular pipe, while our results are for horizontal rectangular duct flow.

The premise that there is a behaviour change can easily be seen by consideration of the friction velocity values. Fig 6 demonstrates that for both of the Reynolds numbers studied here, the average friction velocity decreases significantly compared to the linear extrapolation at about 3 m/s. Below this value, the friction velocities both appear to increase linearly with a similar gradient as the gas velocity increases although a non-linear increase is possible since there are only three points in each line. Above a threshold, the average friction velocity decreases. This can be investigated in more detail by using POD filtering to look at the instantaneous friction velocities.

3.2 POD Analysis of the flow.

To further understand the potential vorticity noted near the trough of the waves, it was decide to attempt POD analysis to filter out the PIV outliers. The snapshot technique was used to produce 2000 modes that could be recombined to recreate the original image, or only partially recombined to produce an approximation. Fig. 7a shows the cumulative energy coefficient of the two cases shown in Fig.3 and 4. In both cases the first mode is the mean. This is not always the case, for example in Wee (2015), the first two modes were the fundamental frequency of oscillation and the 3rd or the 4th mode were the mean depending on the non-linear motions generated by the acoustic field. For the 2D case the mean contains 95% of the energy and the remaining modes only contain 5%. In other words, the flow is mainly stationary. There is a change in gradient at about 10 modes, which is consistent with the transition from signal to random noise. For the 3D wave, the mean is not stationary, so the average energy is lower, about 79.5%. More modes are necessary in this case to recreate the mode with over 90% of the energy.

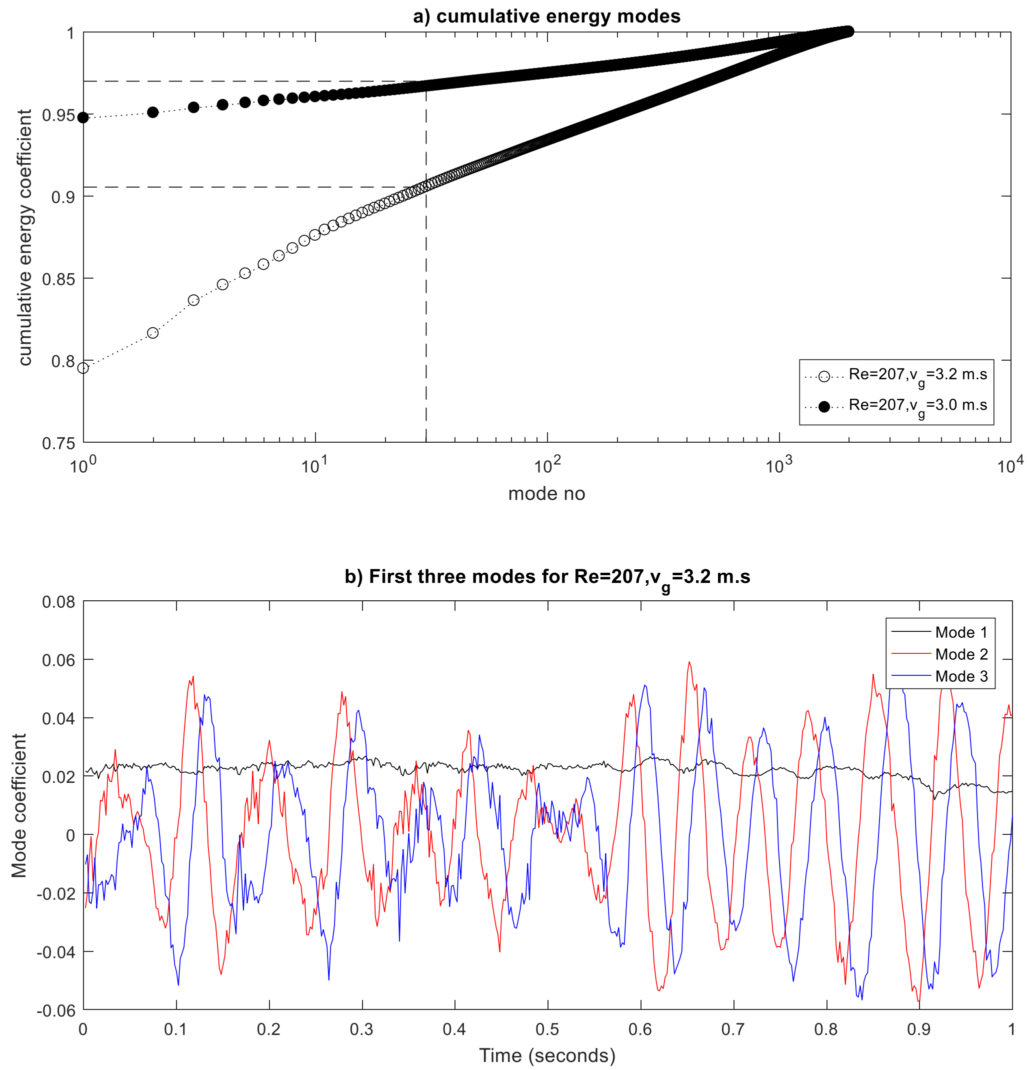

Fig. 7: (a) Energy of POD modes for two cases as identified on graph. The first three modes for one of these cases.

While the average energy of the modes is decreasing as you increase the mode number, this does not mean that the modes are insignificant. Fig 7b shows that the 2nd and 3rd mode of the 3D case have instantaneous magnitudes that are larger than the mean. When recombining, it is necessary to include all such modes. For this recreation, it was decided to take 30 modes, which corresponded to 90% of the energy for the 3D case and 97% of the energy in the 2D case. This cut-off included all modes with significant instantaneous magnitude.

Fig. 8a shows the POD filtered velocity map for the 2D case with 97% of the energy (30 modes). It is clear that much of the random PIV noise and outliers are "averaged" out of the flow. It is now

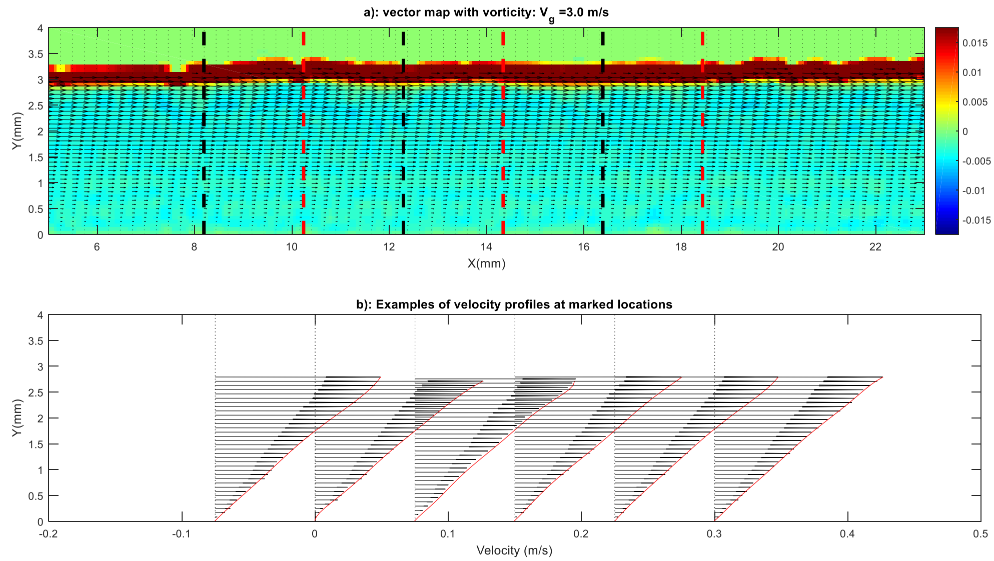

Fig. 8 (a) POD filtered image for Re=207 and v_g = 3.0 m/s. Vorticity is overlaid. Only every second PIV vector is displayed. (b) Velocity profiles at lines indicated in (a). Note vertical scale is stretched.

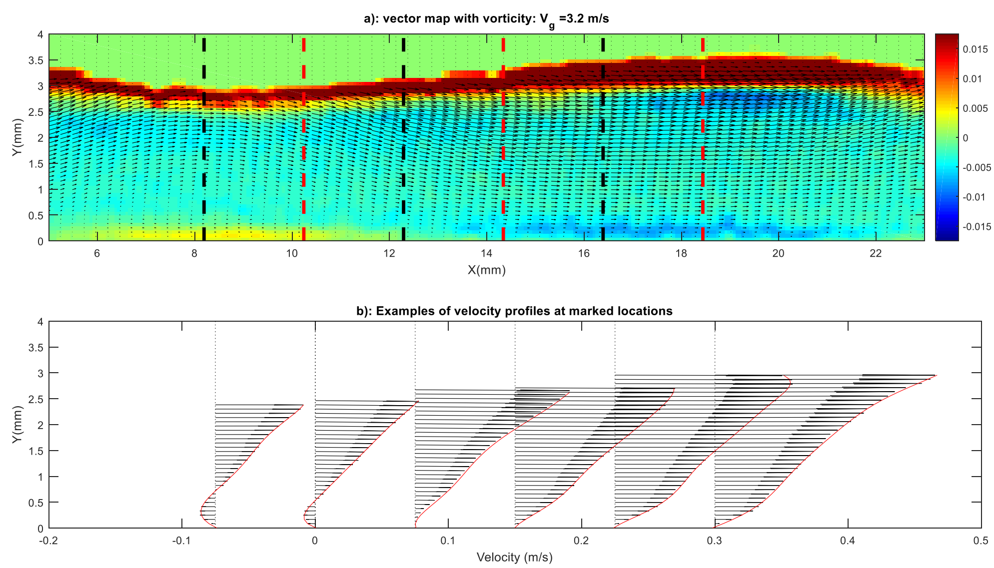

Fig. 9 (a) POD filtered image for Re=207 and v_g = 3.2 m/s. Vorticity is overlaid. Only every second PIV vector is displayed. (b) Velocity profiles at lines indicated in (a). Note vertical scale is stretched

more obvious the velocity field in this case is an oscillating linear profile (Fig 8b). As the 2D surface waves pass by, the linear profile gradient oscillates slightly.

When the air velocity is increased from 3.0 to 3.2 m/s, the flow profile under the wave changes drastically and this can be seen much more clearly when only the 30 modes are included for 90% of the energy in Fig. 9a. The vertical regions near the wall in the region of the wave trough are

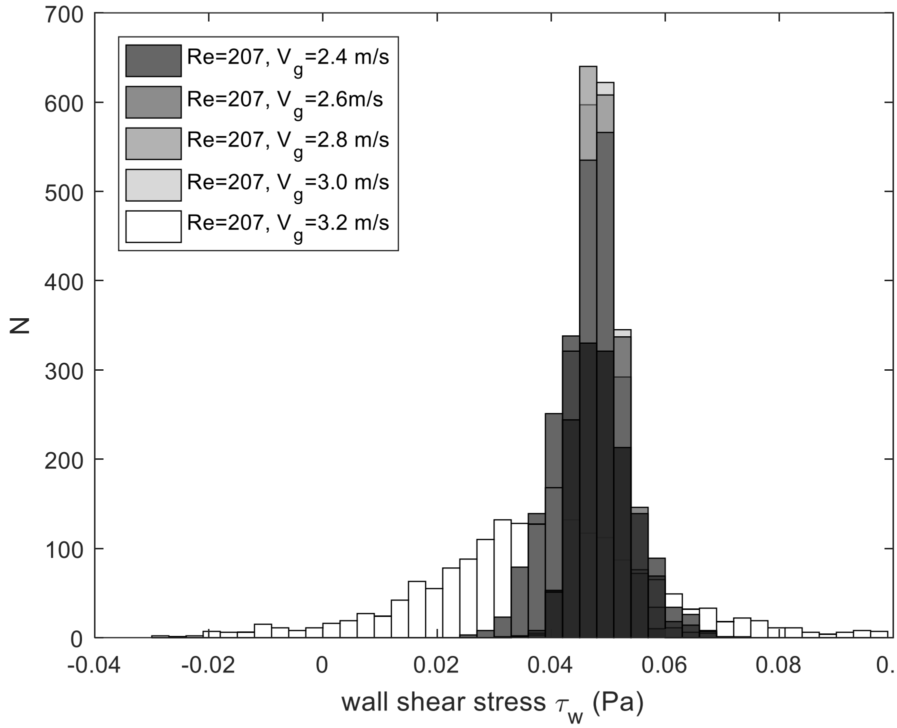

Fig. 10 A comparison of the histograms of the instantaneous wall shear stress for $Re = 207$. For $v_g = 3.2\mathrm{m/s}$, the wall shear stress distribution is much wider and goes to negative values.

now very clear, and it is now also possible to see that they are matched with negative vorticity near the wall and near the surface when a wave crest passes. This is significant, because it means that, unlike in the 2D case, where the wall gradients are fairly constant, in the 3D case the local wall gradients vary significantly and can become negative.

A review of the literature shows that this reversal of flows and negative wall shear stress has been seen in churn flow in upward co-current applications (Kaji and Azzopardi, 2010). However, we are not aware of any results that have seen this in annular flow regimes, although backflow has been noted in falling liquid films (Dietze et al., 2008; Dietze et al., 2014; Tihon et al., 2003). Since wall shear stress and heat transfer are linked, the reversal of the wall shear stress has implications for understanding the heat transfer in application for sheared flow such as in heat exchangers for nuclear and gas powered generation electricity plants.

The POD filtering has produced a smooth transition close to the wall. We are interested in the instantaneous wall shear stress, so a 9th order polynomial is fitted to the velocity profile at the six profiles identified in Fig 9b, and the gradient of this curve at the wall is calculated for the curve

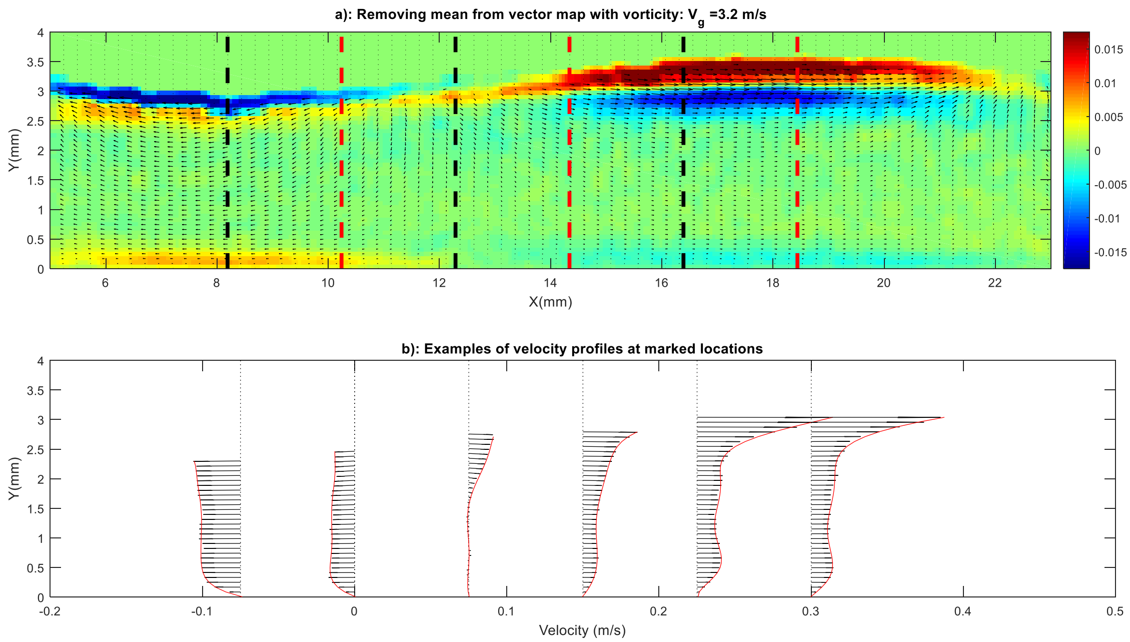

Fig. 11 A POD reconstruction of Re=207 and $v_g = 3.2\mathrm{m/s}$ where only modes 2-30 are included. This emphasises flow reversal.

fit. This was completed for all cases under consideration and the results for $Re = 207$ are shown in Fig. 10. Considering this result in comparison to Fig 9b, it can be deduced that the wall shear stress is larger under the waves and negative under the trough to produce a net value that is positive but lower. The interfacial gradient is also higher under the wave crest and this indicates that the force at that location is accelerating the fluid in the wave. This tallies with the increases wall shear stress under the wave crest. A possibility is that the flow reversal in the trough is due to continuity. The average fluid passing a point must be a constant, so if more is pushed through, then there must be balance.

Another clear possibility is that the flow is in three dimensions and contains an out of plane component, so there is a net flow into the plane at that point from out-of-plane. Some visualisation of the velocity in a horizontal plane close to the wall was also carried out, but the results are not shown here. In this visualisation, oscillating motions across the duct was clearly seen when the gas velocity was larger than $3\mathrm{m/s}$, while the motion of the particles was purely along the duct at lower velocities supporting this idea.

The relative gradients in the wave can more easily be seen if the first order mode is discounted and the POD modes reconstructed using only modes 2 to 30. Fig. 11 shows this for the same case as Fig. 9. This demonstrates that in the trough of the wave there is an almost constant back flow, in comparison to the average velocity profile, while at the wave crest, there is a clear stretching of the fluid as the crest is pushed forward faster than the fluid column below, leading to a net forward flow under the crest.

3.3 POD statistics

One interesting feature from Fig. 7b is that the coefficient of the mode 1 vector is not a fixed constant, but varies with time. Mode 1 is the mean velocity field. The small variations in the pumping speed, or instabilities in the flow result in this linear gradient varying with time. This feature has ramifications in the understanding of the turbulent statistics. Fig. 12 shows how the coefficient associated with the mean varies over the 4 seconds of the experiment. This varied by almost 10% which has implications for calculation of the turbulent statistics. While this variation will produce a 0.2 % uncertainty to the mean value (to 95% confidence level), the turbulent fluctuations are calculated by removing this mean value averaged across all the velocity maps.

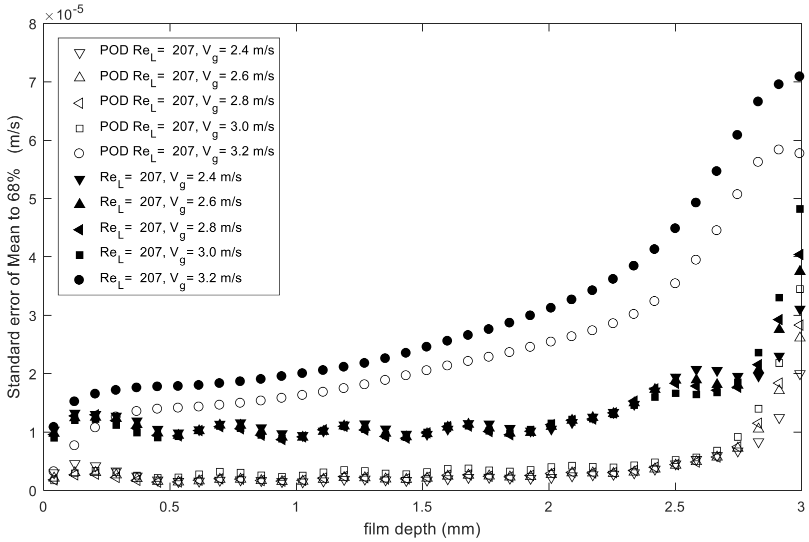

Fig. 13 The standard error of the mean calculate to a 68% confidence level for the original data and the POD filtered (30 modes) data. In all cases the filtered data has a lower uncertainty in the mean.

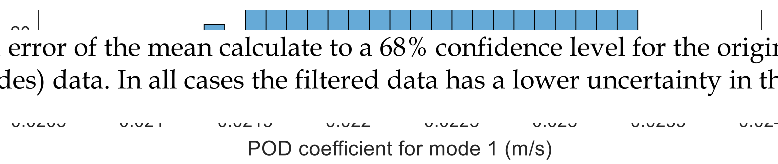

Fig. 12 The variation of the coefficient of the mode corresponding to the mean for Re=166, $v_g = 3.2$ m/s. This varies by almost 10% over the course of the experiment.

Additionally the random PIV noise will also affect the measured turbulent statistics. Many of the POD modes are there to compensate for outlier values. If only one velocity map has a strong outlier at one location, there must be a mode or combination of modes that include that value. Since this occurs very rarely, this mode will be of low energy and will most likely occur only in the higher modes. These higher order modes have clear normal distributions and are uncorrelated to major events and so will only contribute to the addition of noise to the signal of interest. These outliers are, in general larger than "real" results and will act to increase the statistical values calculated.

The noise will statistically decay with energy, and this is why the change in slope of the energy of the modes shown in Fig 7a is one of the criteria needed to ascertain important modes for inclusion. Fig. 13 compares the standard error of the mean profile calculated from the original data and the POD filtered data. This was calculated using

$$\text{SEM to 68\% confidence} = \frac{\sigma(x)}{\sqrt{N-1}}$$

where $\sigma(x)$ is the standard deviation of the data at that height above the wall and N is the number of points used for the average.

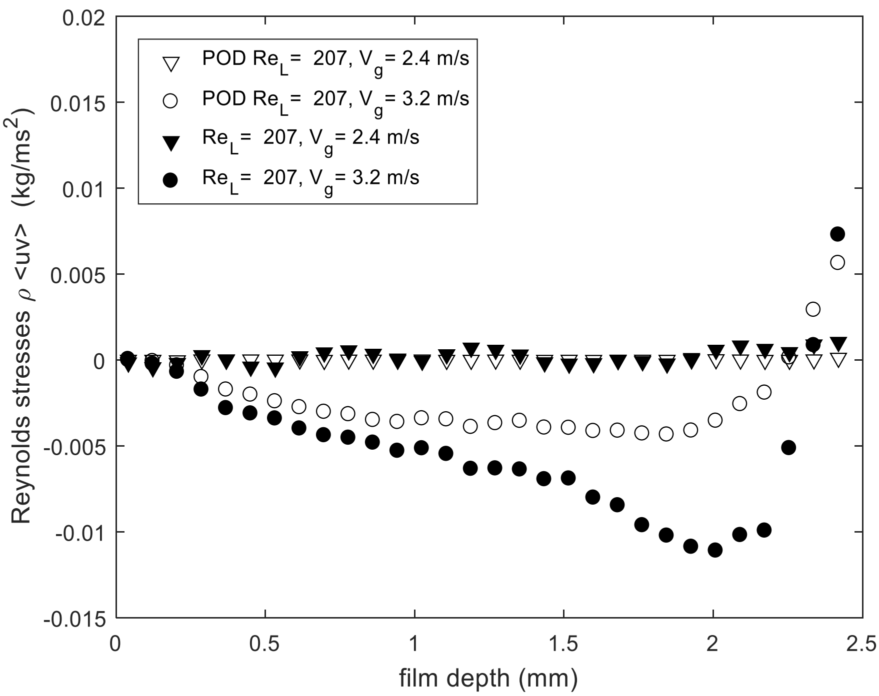

Fig. 14 The comparison of the Reynolds stresses calculated with POD filtering and from the original data.

The figure demonstrates that, while the mean calculated is the same in both cases, the uncertainty in it is decreased. At the lower values, where the flow is 2D, the POD filtered uncertainty in the mean is almost negligible. We would argue that much of the difference is in the magnitude of the PIV noise. In these cases, only 3% of the energy is disregarded in the filtering. For the 3D wave case, there is a decrease in the uncertainty as well, but in this case the uncertainty changes with height from the wall. This is because the flow is oscillating in the 3D mode and the oscillation amplitude increases with distance from the wall.

In addition to the uncertainty in the mean, the PIV noise will also produce an over-prediction of the Reynolds stresses defined as $\rho < uv >$, where u and v and the fluctuating components after subtraction of the mean. Fig. 14 shows that for the 2D case, there are only very small Reynolds stresses and there is almost no difference in the POD and raw data statistics. However there are significant differences for the 3D case. The POD filtered data has produced overall lower values of Reynolds stresses. For the unfiltered data, the stresses increase almost linearly.

4. Conclusions

The transition between 2D and 3D flow in a horizontal rectangular duct has been studied using a PIV technique. To overcome issues with the noise level, a POD filtering technique has been implemented to simplify the identification of the vortex motions near the wall in the duct. The runs were filtered so that the reconstructed modes contained between 90 and 97 % of the total energy.

The filtering demonstrates the change in flow behavior when the waves transition from 2D waves to 3D waves. As the waves become 3D, the amplitude of the waves increase and the shearing motions under the crest increase. In the region below the trough, a flow reversal can be seen which could either be a feature of continuity or the interaction of an overlapping wave out of plane.

The transition also leads to a change in the average wall shear stress. As the air flow increases above 3 m/s and the flow starts to change from 2D to 3D, there is a significant decrease in the average wall shear stress. In fact it is shown that the instantaneous shear stress can even become negative. It can also be seen that the so called laminar region extends further than in classic wall pipe flows. Similar to other previous results, the linear region extends to $y^+ \sim 10$. This can have implication for dealing with wall boundary conditions in CFD or in heat transfer studies.

Finally it is shown that the POD filtering can reduce the level of noise in the signal, although more thought needs to be put into to address the correct level of POD filtering to get optimal statistics.

References

André, M.A., Bardet, P.M., 2015. Interfacial shear stress measurement using high spatial resolution multiphase PIV. Experiments in Fluids 56.
Ashwood, A.C., Vanden Hogen, S.J., Rodarte, M.A., Kopplin, C.R., Rodríguez, D.J., Hurlburt, E.T., Shedd, T.A., 2015. A multiphase, micro-scale PIV measurement technique for liquid film velocity measurements in annular two-phase flow. International Journal of Multiphase Flow 68, 27-39.
Ayati, A.A., Kolaas, J., Jensen, A., Johnson, G.W., 2014. A PIV investigation of stratified gas–liquid flow in a horizontal pipe. International Journal of Multiphase Flow 61, 129-143.
Ayati, A.A., Kolaas, J., Jensen, A., Johnson, G.W., 2015. Combined simultaneous two-phase PIV and interface elevation measurements in stratified gas/liquid pipe flow. International Journal of Multiphase Flow 74, 45-58.
Cherdantsev, A.V., Hann, D.B., Azzopardi, B.J., 2014. Study of gas-sheared liquid film in horizontal rectangular duct using high-speed LIF technique: Three-dimensional wavy structure and its relation to liquid entrainment. International Journal of Multiphase Flow 67, 52-64.
Cioncolini, A., Del Col, D., Thome, J.R., 2015. An indirect criterion for the laminar to turbulent flow transition in shear-driven annular liquid films. International Journal of Multiphase Flow 75, 26-38.

Dietze, G.F., Leefken, A., Kneer, R., 2008. Investigation of the backflow phenomenon in falling liquid films. Journal of Fluid Mechanics 595, 435-459.
Dietze, G.F., Rohlfs, W., Nährich, K., Kneer, R., Scheid, B., 2014. Three-dimensional flow structures in laminar falling liquid films. Journal of Fluid Mechanics 743, 75-123.
Graftieaux, L., Michard, M., Nathalie, G., 2001. Combining PIV, POD and vortex identification algorithms for the study of unsteady turbulent swirling flows. Measurement Science and Technology 12, 1422-1429.
Kaji, R., Azzopardi, B.J., 2010. The effect of pipe diameter on the structure of gas/liquid flow in vertical pipes. International Journal of Multiphase Flow 36, 303-313.
Ma, X., Schröder, A., 2017. Comparison of signal-based and POD-based phase-averaged Reynolds stress in a perturbed separated shear flow. Journal of Visualization 20, 509-514.
Perrin, R., Braza, M., Cid, E., Cazin, S., Barthet, A., Sevrain, A., Mockett, C., Thiele, F., 2007. Obtaining phase averaged turbulence properties in the near wake of a circular cylinder at high Reynolds number using POD. Experiments in Fluids 43, 341-355.
Schubring, D., Foster, R.E., Rodríguez, D.J., Shedd, T.A., 2009. Two-zone analysis of wavy two-phase flow using micro-particle image velocimetry (micro-PIV). Measurement Science and Technology 20, 065401.
Tihon, J., Tovchigrechko, V., SobolíK, V., Wein, O., 2003. Electrodiffusion detection of the near-wall flow reversal in liquid films at the regime of solitary waves. Journal of Applied Electrochemistry 33, 577-587.
Wee, D.S.T., 2015. PIV investigation of acoustic transmission through curved duct bends for the optimisation of thermoacoustic systems. PhD Thesis. The University of Nottingham Malaysia. http://eprints.nottingham.ac.uk/29312/
Zadrazil, I., Markides, C.N., 2014. An experimental characterization of liquid films in downwards co-current gas-liquid annular flow by particle image and tracking velocimetry. International Journal of Multiphase Flow 67, 42-53.